Low-loss Ge-rich Si0.2 Ge0.8 waveguides for mid-infrared photonics

Joan-Manel Ramirez, Vladyslav Vakarin, Clement Gilles, Jacopo Frigerio, Andrea Ballabio, Papichaya Chaisakul, Xavier Le Roux, Carlos Alonso-Ramos, Gregory Maisons, Laurent Vivien, et al.

Low-loss Ge-rich $Si_{0.2}Ge_{0.8}$ waveguides for mid-infrared photonics

JOAN MANEL RAMIREZ,[1,*,+] VLADYSLAV VAKARIN,[1,+] CLEMENT GILLES,[2] JACOPO FRIGERIO,[3] ANDREA BALLABIO,[3] PAPICHAYA CHAISAKUL,[1] XAVIER LE ROUX,[1] CARLOS ALONSO-RAMOS,[1] GREGORY MAISONS,[2] LAURENT VIVIEN,[1] MATHIEU CARRAS,[2] GIOVANNI ISELLA,[3] AND DELPHINE MARRIS-MORINI[1]

[1]*Centre de Nanosciences et de Nanotechnologies, Université Paris Sud, CNRS, Université Paris Saclay, 91405 Orsay, France.*
[2]*MirSense, 86 Rue de Paris, 91400 Orsay, France.*
[3]*L-NESS, Dipartimento di Fisica, Politecnico di Milano, Polo di Como, Via Anzani 42, 22100 Como, Italy.*

**Corresponding author: joan-manel.ramirez@u-psud.fr* *[+]Both authors contributed equally to this work*

Received XX Month XXXX; revised XX Month, XXXX; accepted XX Month XXXX; posted XX Month XXXX (Doc. ID XXXXX); published XX Month XXXX

We demonstrate low-loss Ge-rich $Si_{0.2}Ge_{0.8}$ waveguides on $Si_{1-x}Ge_x$ (x from 0 to 0.79) graded substrates operating in the mid-infrared wavelength range, at λ = 4.6 μm. Propagation losses as low as (1.5 ± 0.5) dB/cm and (2 ± 0.5) dB/cm were measured for the quasi-TE and quasi–TM polarizations, respectively. Total coupling loss (input/output) of only 10 dB was found for waveguide widths larger than 7 μm due to a good fiber-waveguide mode matching. Near-field optical mode profiles measured at the output waveguide facet allowed to inspect the optical mode and precisely measure the modal effective area of each waveguide providing a good correlation between experiments and simulations. These results put forward the potential of low-index-contrast $Si_{1-x}Ge_x$ waveguides with high Ge concentration as fundamental blocks for mid-infrared photonic integrated circuits.

OCIS codes: (130.0130) Integrated optics, integrated optics materials, infrared; (230.0230) Optical devices, Waveguides; (220.0220) Optical design and fabrication.

http://dx.doi.org/10.1364/OL.99.099999

Mid-infrared photonic integrated circuits (mid-IR PICs) are recently gaining significance due to the vast number of applications foreseen over the 2-20 μm wavelength range [1]. Among them, the use of mid-IR on-chip approaches as enabling systems to develop ultra-sensitive label-free and compact spectroscopic sensors is driving much of the expectations for this new platform [2-6]. The concept relies on the exploitation of the strong mid-IR absorption present in several substances and molecules to detect tiny analyte concentrations, potentially parts per billion (ppb). Alternatively, the use of mid-IR PICs has also been proposed as a powerful solution to several major drawbacks existing in other important areas such as thermal imaging, free-space optical communications, astronomy or medical diagnostics [7, 8].

In that regard, Si-based technologies have shown great potential for the implementation of new mid-IR PICs, following a natural trend motivated by the large pool of devices already demonstrated at telecom wavelengths [9]. The possibility to use a mature technology combined with the suppression of silicon's two-photon absorption (TPA) in the mid-IR is also considered as a crucial advantage to realize novel nonlinear devices for supercontinuum generation or frequency conversion, among others [10, 11]. Nevertheless, the conventional SOI platform typically used for near-infrared (NIR) integrated optical platforms poses challenges for mid-IR integration, as the SiO_2 experiences an early absorption in the mid-IR starting around λ ~ 3.6 μm. In order to overcome this limitation, several works have suggested implementations of mid-IR silicon-based platforms that outperform SOI performance by using Si-on-saphire (SOS), Si-on-Si nitride (SON), Si-on-porous Si, suspended Si, Ge-on-Si or SiGe-on-Si [12-25]. The latest approach is particularly interesting since it allows fine control of the material properties such as the bandgap or the refractive index by balancing the Ge concentration in the alloy, while extending the operation range up to at least 8 μm (Si absorption onset), with possibility to further extend it to 14 μm (Ge transparency cut-off wavelength) for devices with low Si concentration. Moreover, Ge presents higher nonlinear properties than Si and a TPA cut-off at λ ~ 3.2 μm, hence making Ge-rich structures a convenient choice to develop nonlinear optical devices in the mid-IR [26].

In this work, we demonstrate low-loss Ge-rich $Si_{0.2}Ge_{0.8}$ rib waveguides on $Si_{1-x}Ge_x$ graded substrates operating at 4.6 μm. Such passive structures could be used as an elemental building block to develop more complex mid-IR PICs. It is worth noting that although other works have already reported low-loss $Si_{1-x}Ge_x$ waveguides in the mid-IR, they used lower Ge concentrations at the waveguide core (x < 0.5) and a Si cladding that limited the

operation wavelength at $\lambda < 8$ μm [25, 27]. Instead, the waveguides used here are based on a higher Ge content in the guiding core ($x \sim 0.8$) and a Si-cladding-free design that may allow to further extend the operation wavelength beyond the Si absorption onset.

The epilayer was deposited using Low Energy Plasma Enhanced Chemical Vapor Deposition (LEPECVD). A graded $Si_{1-x}Ge_x$ substrate with a linear increase of the Ge concentration up to $x = 0.79$ was first grown at a rate of 5-10 nm/s over commercial Si (001) wafers, with a total thickness of 11 μm. A 2 μm thick $Si_{1-x}Ge_x$ layer with constant Ge concentration of $x = 0.8$ was then grown on top of the graded buffer to be used as guiding layer. Such approach allows to efficiently reduce the number of threading dislocations (TDD) to $3x10^6$ cm^{-2} by gradual accommodation of the Si-Ge lattice mismatch in the layer stack [28]. The surface roughness of the top layer is 3.5 nm rms as measured by AFM. The compositional mismatch between the top layer and the graded buffer generates a small refractive index step in the waveguide core, which helps to confine the optical mode [29, 30]. Rib waveguides of different widths (4, 5, 6, 7 and 8 μm) and different lengths (3, 4, 5 and 6 mm) were defined by etching the Ge-rich $Si_{0.2}Ge_{0.8}$ layer down to 1.5 μm using Inductively Coupled Plasma (ICP) technique. Hydrogen peroxide solution (H_2O_2) was used to smooth the sidewall roughness. The inset of figure 1 shows a schematic cross-section of the waveguides that have been fabricated and characterized. An additional deep etching step (down to ~120 μm) was performed to define the waveguide facets and to allow an easy placement of the input fiber close to the waveguide's input facet. The sample design is seen in the SEM picture of Figure 1, showing the deep-etch step to obtain the different straight waveguide lengths from 3 to 6 mm long. Additionally, a zoomed view over single waveguides (top images in figure 1) allowed to corroborate the good agreement between waveguide dimensions and the nominal design, with an uncertainty of ± 0.2 μm. Smooth waveguide facets and reasonable low sidewall roughness were also observed.

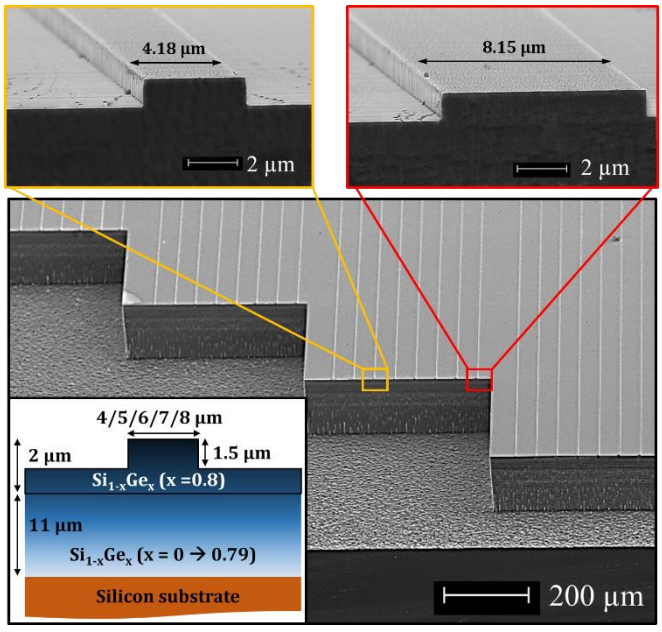

Fig. 1. SEM pictures of Ge-rich $Si_{0.2}Ge_{0.8}$ rib waveguides with facets defined by deep ICP etching. The top images display a zoomed view of a waveguide with a nominal width of 4 μm (left) and 8 μm (right), respectively. The inset figure represents a simplified schematic of the waveguide cross-section.

A cut-back technique was then used to characterize optical loss of the waveguides in a non-destructive manner, with no need of sequential cleaving and further polishing of the waveguide facet after each measurement.

Waveguide characterization was performed using (i) a quantum cascade laser (QCL) operating at 4.6 μm coupled to a mid-IR single mode micro-structured optical fiber for waveguide butt-coupling with (ii) a free-space mid-IR collection system using a plano-convex lens aligned with a mid-IR thermal camera. In the absence of polarization-maintaining mid-IR optical fibers, an optical polarizer was placed at the waveguide output facet to filter quasi-TE and quasi-TM polarizations. The measured power at the fiber output was limited at 0.5 mW, a value low enough to avoid the influence of nonlinear effects. The near-field optical modes were monitored in real time by the mid-IR camera and integrated all over the waveguide facet. Low propagation losses were measured, which are nearly independent from the waveguide width, as shown in Figure 2. The measured transmission values of the 7 μm-width waveguides are reported using circles for TE modes and squares for TM modes, while the vertical bars illustrate the experimental error deviation. Finally low-loss optical mode propagation is obtained for both polarizations, corresponding to (1.5 ± 0.5) dB/cm and (2 ± 0.5) dB/cm for the quasi-TE and quasi-TM modes, respectively, with almost no dependence on the waveguide width. It is worth to remark that although Finite Difference Method (FDM) simulations denoted multimodal behavior in waveguides wider than 5 μm for the current operating wavelength, in practice only the first mode was observed at the output facet of waveguides. This may be explained considering that higher order modes normally present higher coupling losses. Therefore, we can assume that only the first mode was propagated and no significant mode-beating nor mode-coupling occurred in the waveguides.

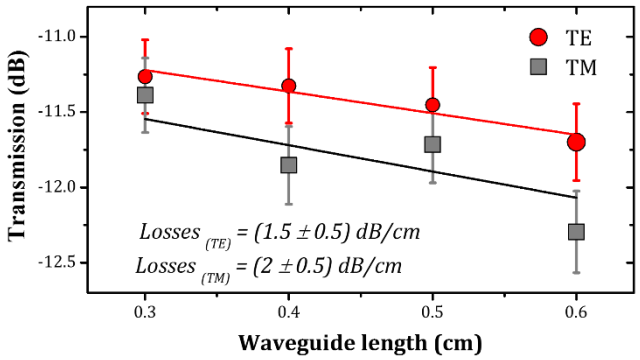

Fig. 2. Representative transmission measurements of Ge-rich $Si_{0.2}Ge_{0.8}$ waveguides as a function of the waveguide length for the quasi-TE (red dots) and the quasi-TM (grey squares) optical modes. The squares and circles correspond to the measurement of the 7 μm-width waveguides while the vertical bars illustrate the experimental error deviation. Finally solid lines correspond to the linear fitting of experimental data to deduce the losses per length unit.

Apart from propagation losses, the coupling losses in and out of the waveguides have been investigated. To this purpose, the evolution of the transmitted optical signal (taking into account

coupling and propagation losses) as a function of the waveguide width has been drawn in Figure 3 for a waveguide length of 6 mm. While the measured transmission takes into account both coupling and propagation losses, it can be noted that the contribution from propagation losses is roughly estimated around 1 dB from previous results, and so the measured total losses which are comprised between ~ 10 and 14 dB come mostly from the coupling losses.

A linear decrease of the coupling losses is observed for increasingly wide waveguides, with a subsequent saturation trend for the widest designs (widths of 7 and 8 μm) around a transmission value of ~-10 dB. The origin of this trend may be attributed to a smaller mode mismatch for wider waveguides.

In order to corroborate this hypothesis, the near-field optical mode profile was recorded at the output of each waveguide facet and compared with the one obtained at the fiber output directly. Results are displayed at the inset images of Figure 3. As seen, an evident difference in size (over 25 %) is observed between the optical modes of waveguides having a width of 4 μm (left hand side inset) and 7 μm (middle inset), being the latest one comparable to the measured near-field optical mode of the fiber (right hand side inset).

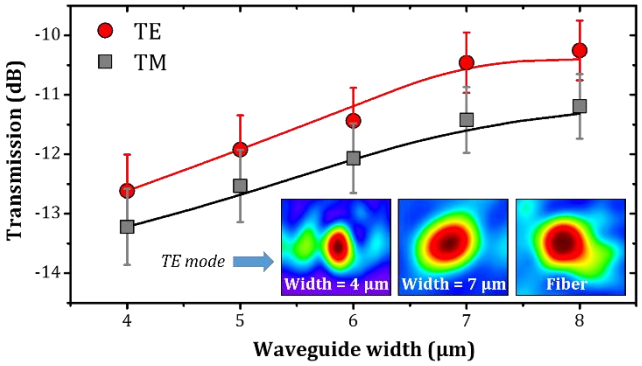

Fig. 3. Total measured optical transmission (including coupling and propagation losses, y-axis) of Ge-rich $Si_{0.2}Ge_{0.8}$ rib waveguides with a length of 6 mm and variable widths from 4 μm to 8 μm (x-axis). The insets show the recorded near-field optical mode profiles (in false colors) of the waveguide 4 μm wide (left hand side), 7 μm wide (middle) and the optical fiber (right hand side).

Further modal analysis in waveguides was performed by calculating the modal effective area (A_{eff}) of recorded optical modes and comparing it with the simulated trend obtained from the mode solver software. The main results are shown in Figure 4, denoting a good agreement between measurements and simulations for both polarizations. Such accurate reproducibility of the experimental results validates our simulations methodology on graded-index designs and provides a solid baseline to simulate more complex structures with different Ge gradient concentration profiles. Insets at the bottom-right hand side of Figure 4 compare the simulated (left) and measured (right) quasi-TE near-field optical mode profiles of a 7 μm wide waveguide. The measured optical mode presents an aberration that deforms its shape, caused by the collection optics. As can be observed, a considerable fraction of the optical mode penetrates into the $Si_{1-x}Ge_x$ graded substrate, with no major consequences. Indeed, the gradual refractive index increase defined in the graded substrate provides sufficient vertical contrast to maintain the mode well confined in the waveguide. A gradual increase of the A_{eff} is observed for wider waveguides, as expected. Remarkably, an inflection point seems to take place towards narrower waveguides, especially for the quasi-TE mode, which could be explained by considering the mode de-confinement in the waveguide when its width is reduced. Reducing the waveguide width to less than 4 μm compromises the mode fitting inside the rib area. Consequently, the propagating mode is pulled downwards in the waveguide, hence diminishing the lateral confinement of the optical modes. To better illustrate this effect, insets at the top-left hand side of figure 4 show a modal comparison between the simulated quasi-TE mode of a narrow waveguide 3.5 μm wide with another one 8.5 μm wide (extreme values of Figure 4). A clear deformation of the optical mode is observed for the narrowest waveguide caused by the aforementioned lateral de-confinement. Moreover, this interpretation is also consistent with the slightly better mode confinement simulated for the quasi-TM mode, since this polarization is less sensitive to lateral confinement.

Therefore, the last two figures have shown interesting features that should be considered when implementing Ge-rich $Si_{1-x}Ge_x$ waveguides for future mid-IR applications. For instance, when designing nonlinear optical devices operating at this wavelength, optimum input coupling performance is desired to maximize the coupled power inside the structures, and therefore wide waveguides (> 7 μm) may be used. However, tight mode confinement is also crucial for nonlinear photonics, hence being the narrow designs the most appropriate to carry out this task. To address this contradictory constraint, a trade-off between both scenarios may be conducted either by choosing an intermediate design (i. e. a width of ~ 6 μm in this case) or by combining wide sections for efficient input coupling condition with narrower ones to boost the nonlinear effects in the Ge-rich guiding core.

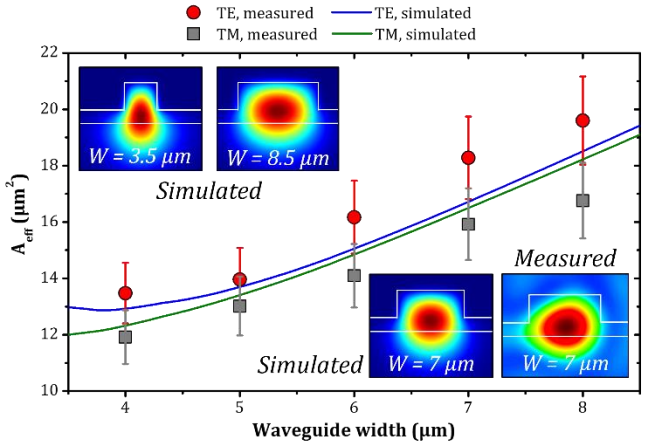

Fig. 4. Comparison between the measured (dotted and squared data) and simulated (solid lines) modal effective area of the quasi-TE mode (red dots and blue line) and the quasi-TM mode (grey squares and green line) as a function of the waveguide width for an operating wavelength of λ = 4.6 μm. Right-bottom insets display a modal comparison between the simulated (left) and measured (right) quasi-TE mode profiles of the 7 μm wide waveguide. Inset images at the upper-left hand side show the simulated quasi-TE near-field mode profile of a 3.5 μm (left) and a 8.5 μm (right) wide waveguide.

In summary, low-loss Ge-rich $Si_{0.2}Ge_{0.8}$ rib waveguides on graded $Si_{1-x}Ge_x$ (x from 0 to 0.79) substrates have been demonstrated at a

wavelength of 4.6 μm. Propagation losses for quasi-TE and quasi–TM modes have been inspected by cut-back technique, obtaining a value of (1.5 ± 0.5) dB/cm and (2 ± 0.5) dB/cm, respectively. In addition, the total coupling loss as a function of the waveguide width has been studied, obtaining an optimum mode-matching condition for waveguides wider than 7 μm that provides an average coupling loss of ~10 dB. Finally, the evolution of the modal effective area upon increase of the waveguide width has also been examined by integrating the measured near-field optical mode at the output of the waveguide facet, obtaining a good correlation between experiments and simulations.

Funding. The fabrication of the device was performed at the nano-center CTU-IEF-Minerve, which is partially funded by the "Conseil Général de l'Essonne". This work was partly supported by the French RENATECH network. D.M-M. acknowledges support by the Institut Universitaire de France. This project has received funding from the European Research Council (ERC) under the European Union's Horizon 2020 research and innovation programme (grant agreement N°639107-INsPIRE).

References

1. R. Soref, Nature Photonics, **4**, 495 (2010).
2. X. Wang, S. S. Kim, R. Roßbach, M. Jetter, P. Michler, and B. Mizaikoff, Analyst, **137**, 2322 (2012).
3. Y. C. Chang, P. Wägli, V. Paeder, A. Homsy, L. Hvozdara, P. van der Wal, J. Di Francesco, N. F. de Rooij, and H. P. Herzig, Lab on a Chip, **12**, 3020 (2012).
4. J. Haas, B. Mizaikoff, Annual Review of Analytical Chemistry, **0** (2016).
5. P. T. Lin, V. Singh, J. Hu, K. Richardson, J. D. Musgraves, I. Luzinov, J. Hensley, L. C. Kimerling, and A. Agarwal, Lab on a Chip, **13**, 2161 (2013).
6. Y. Zou, S. Chakravarty, P. Wray, and R. T. Chen, Sens. Actuator B-Chem. **221**, 1094 (2015).
7. J. Hu, J. Meyer, K. Richardson, and L. Shah, **3**, 1571 (2013).
8. M. Nedeljkovic, A. Z. Khokhar, Y. Hu, X. Chen, J. S. Penades, S. Stankovic, H. M. H. Chong, D. J. Thomson, F. Y. Gardes, G. T. Reed, and G. Z. Mashanovich, Opt.Mater.Express **3(9)**, 1205 (2013).
9. L. Vivien, and L. Pavesi, (Eds.). Handbook of silicon photonics. Taylor & Francis (2016).
10. B. Kuyken, X. Liu, R. M. Osgood, R. Baets, G. Roelkens, W. M. Green, Optics Express, **19**, 20172 (2011).
11. S. Zlatanovic, J. S. Park, S. Moro, J. M. C. Boggio, I. B. Divliansky, N. Alic, S. Mookherjea, and S. Radic, Nature Photonics, **4**, 561 (2010).
12. N. Singh, D. D. Hudson, Y. Yu, C. Grillet, S. D. Jackson, A. Casas-Bedoya, A. Read, P. Atanackovic, S. G. Duvall, S. Palomba, B. Luther-Davies, S. Madden, D. J. Moss, and B. J. Eggleton, Optica, **2**, 797 (2015).
13. Y. Zou, H. Subbaraman, S. Chakravarty, X. Xu, A. Hosseini, W.-C. Lai, P. Wray, and R. T. Chen, Optics Letters, **39**(10), 3070 (2014).
14. S. Khan, J. Chiles, J. Ma, and S. Fathpour, Applied Physics Letters, **102**, 121104 (2013).
15. G. Z. Mashanovich, M. M. Milošević, M. Nedeljkovic, N. Owens, B. Xiong, E. J. Teo, and Y. Hu, Optics Express, **19**, 7112 (2011).
16. P. T. Lin, V. Singh, Y. Cai, L. C. Kimerling, and A. Agarwal, Optics Letters, **38**(7), 1031 (2013).
17. X.Wang, Z. Cheng, K. Xu, H. K. Tsang, and J.-B. Xu, Nature Photon. **7**, 888 (2013).
18. J. Soler Penadés, A. Ortega-Moñux, M. Nedeljkovic, J. G. Wangüemert-Pérez, R. Halir, A. Z. Khokhar, C. Alonso-Ramos, Z. Qu, I. Molina-Fernández, P. Cheben, and G. Z. Mashanovich, Opt. Express **24**, 22908 (2016).
19. Y. C. Chang, V. Paeder, L. Hvozdara, J. M. Hartmann, and H. P. Herzig, Optics letters, **37**, 2883 (2012).
20. A. Malik, M. Muneb, Y. Shimura, J. V. Campenhout, R. Loo, and G. Roelkens, IEEE Photon. Technol. Lett. **25**(18), 1805 (2013).
21. A. Malik, S. Dwivedi, L. Van Landschoot, M. Muneeb, Y. Shimura, G. Lepage, J. Van Camperhout, W. Vanherle, T. Van Opstal, R. Loo, and G. Roelkens, Optics Express, **22**(23), 28479 (2014).
22. P. Barritault, M. Brun, P. Labeye, J.-M. Hartmann, F. Boulila, M. Carras, and S. Nicoletti, Optics Express, 23(20), 26168 (2015).
23. M. Nedeljkovic, J. Soler Penades, C. J. Mitchell, A. Z. Khokhar, S. Stankovic, T. Dominguez Bucio, C. G. Littlejohns, F. Y. Gardes, and G. Z. Mashanovich, IEEE Photon. Technol. Lett. **27**(10), 1040 (2015).
24. B. Troia, J. S. Penades, A. Z. Khokhar, M. Nedeljkovic, C. Alonso-Ramos, V. M. N. Passaro, G. Z. Mashanovich, Optics Letters, **41**(3), 610 (2016).
25. M. Brun, P. Labeye, G. Grand, J. M. Hartmann, F. Boulila, M. Carras, and S. Nicoletti, Optics express, **22**, 508 (2014). yeah
26. L. Carletti, P. Ma, Y. Yu, B. Luther-Davies, D. Hudson, C. Monat, R. Orobtchouk, S. Madden, D. J. Moss, M. Brun, S. Ortiz, P. Labeye, S. Nicoletti, and C. Grillet, Optics express, **23**, 8261 (2015).
27. L. Carletti, M. Sinobad, P. Ma, Y. Yu, D. Allioux, R. Orobtchouk, M. Brun, S. Ortiz, P. Labeye, J. M. Hartmann, S. Nicoletti, S. Madden, B. Luther-Davies, D. J. Moss, C. Monat, and C. Grillet, Optics express, **23**, 32202 (2015).
28. S. Marchionna, A. Virtuani, M. Acciarri, G. Isella, and H. von Kaenel. Mat. Sci. Semicond. Process. 9 (4–5) 802 (2006).
29. P. Chaisakul, D. Marris-Morini, J. Frigerio, D. Chrastina, M. S. Rouifed, S. Cecchi, P. Crozat, G. Isella, and L. Vivien, Nature Photonics, **8**, 482 (2014).
30. V. Vakarin, P. Chaisakul, J. Frigerio, A. Ballabio, X. Le Roux, J. R. Coudevylle, D. Bouville, D. Perez-Galacho, L. Vivien, G. Isella, and D. Marris-Morini, Optics Express, 23, 30821 (2015).

REFERENCES

1. R. Soref, "Mid-infrared photonics in silicon and germanium," Nature Photonics, 4, 495 (2010).
2. X. Wang, S. S. Kim, R. Roßbach, M. Jetter, P. Michler, and B. Mizaikoff, "Ultra-sensitive mid-infrared evanescent field sensors combining thin-film strip waveguide with quantum cascade lasers," Analyst, 137, 2322 (2012).
3. Y. C. Chang, P. Wägli, V. Paeder, A. Homsy, L. Hvozdara, P. van der Wal, J. Di Francesco, N.F. de Rooij,and H. P. Herzig, "Cocaine detection by a mid-infrared waveguide integrated with a microfluidic chip," Lab on a Chip, 12, 3020 (2012).
4. J. Haas, B. Mizaikoff, "Advances in Mid-infrared Spectroscopy for Chemical Analysis," Annual Review of Analytical Chemistry, 9 (2016).
5. P. T. Lin, V. Singh, J. Hu, K. Richardson, J. D. Musgraves, I. Luzinov, J. Hensley, L. C. Kimerling, and A. Agarwal, "Chip-scale Mid-Infrared chemical sensors using air-clad pedestal silicon waveguides," Lab on a Chip, 13, 2161 (2013).
6. Y. Zou, S. Chakravarty, P. Wray, and R. T. Chen, "Mid-infrared holey and slotted photonic crystal waveguides in silicon-on-saphire for chmical warfare simulant detection," Sens. Actuator B-Chem. 221, 1094-1103 (2015).
7. J.Hu, J.Meyer, K. Richardson, and L. Shah, "Feature issue introduction: mid-IR photonic materials, Optical Materials Express 3(9), 1571(2013)
8. M. Nedeljkovic, A. Z. Khokhar, Y. Hu, X. Chen, J. S. Penades, S. Stankovic, H.M.H. Chong, D.J. Thomson, F.Y. Gardes, G.T.Reed and G. Z. Mashanovich,"Silicon photonic devices and platforms for the mid-infrared," Optical Materials Express 3, 1205 (2013)
9. L. Vivien, and L. Pavesi, (Eds.). Handbook of silicon photonics. Taylor & Francis (2016).
10. B. Kuyken, X. Liu, R. M. Osgood, R. Baets, G. Roelkens, W. M. Green, "Mid-infrared to telecom-band supercontinuum generation in highly nonlinear silicon-on-insulator wire waveguides," Optics Express, 19, 20172 (2011).
11. S. Zlatanovic, J. S. Park, S. Moro, J. M. C. Boggio, I. B. Divliansky, N. Alic, S. Mookherjea and S. Radic, "Mid-infrared wavelength conversion in silicon waveguides using ultracompact telecom-band-derived pump source," Nature Photonics, 4, 561 (2010).
12. N. Singh, D. D. Hudson, Y. Yu, C. Grillet, S. D. Jackson, A. Casas-Bedoya, A. Read, P. Atanackovic , S.G. Duvall, S. Palomba , B. Luther-Davies, S. Madden, D.J.Moss, and B.J. Eggleton, "Midinfrared supercontinuum generation from 2 to 6 μm in a silicon nanowire,"Optica, 2, 797 (2015).
13. Y. Zou, H. Subbaraman, S. Chakravarty, X. Xu, A. Hosseini, W.-C. Lai, P. Wray, and R. T. Chen, "Grating-coupled silicon-on-saphire integrated slot waveguides operating at mid-infrared wavelengths," Optics Letters, 39(10), 3070-3073 (2014).
14. S. Khan, J. Chiles, J. Ma, and S. Fathpour, "Silicon-on-nitride Waveguides for Mid-and Near-infrared Integrated Photonics," Applied Physics Letters, 102, 121104 (2013).
15. G. Z. Mashanovich, M. M. Milošević, M. Nedeljkovic, N. Owens, B. Xiong, E. J. Teo, and Y. Hu,"Low loss silicon waveguides for the mid-infrared," Optics Express, 19, 7112 (2011).
16. P. T. Lin, V. Singh, Y. Cai, L. C. Kimerling, and A. Agarwal, "" Optics Letters, 38(7), 1031 (2013).
17. X.Wang, Z. Cheng, K. Xu, H. K. Tsang, and J.-B. Xu, "High-responsivity graphene/silicon-heterostructure waveguide photodetectors," Nature Photon. 7, 888-891 (2013).
18. J. Soler Penadés, A. Ortega-Moñux, M. Nedeljkovic, J. G. Wangüemert-Pérez, R. Halir, A. Z. Khokhar, C. Alonso-Ramos, Z. Qu, I. Molina-Fernández, P. Cheben, and G. Z. Mashanovich, "Suspended silicon mid-infrared waveguide devices with subwavelength grating metamaterial cladding," Opt. Express 24, 22908-22916 (2016).
19. Y. C. Chang, V. Paeder, L. Hvozdara, J. M. Hartmann, and H. P. Herzig,"Low-loss germanium strip waveguides on silicon for the mid-infrared," Optics letters, 37, 2883 (2012).
20. A. Malik, M. Muneb, Y. Shimura, J. V. Campenhout, R. Loo, and G. Roelkens, "Germanium-on-Silicon Planar Concave Grating Wavelength (de)multiplexers in the mid-Infrared," IEEE Photon. Technol. Lett. 25(18), 1805-1808 (2013).
21. A. Malik, S. Dwivedi, L. Van Landschoot, M. Muneeb, Y. Shimura, G. Lepage, J. Van Camperhout, W. Vanherle, T. Van Opstal, R. Loo, and G. Roelkens, "Ge-on-Si and Ge-on-SOI thermo-optic phase shifters for the mid-infrared," Optics Express, 22(23), 28479-28488 (2014).
22. P. Barritault, M. Brun, P. Labeye, J.-M. Hartmann, F. Boulila, M. Carras, and S. Nicoletti, "Design, fabrication and characterization of an AWG at 4.5 μm," Optics Express, 23(20), 26168-26181 (2015).
23. M. Nedeljkovic, J. Soler Penades, C. J. Mitchell, A. Z. Khokhar, S. Stankovic, T. Dominguez Bucio, C. G. Littlejohns, F. Y. Gardes, and G. Z. Mashanovich, "Surface Grating Coupled Low Loss Ge-on-Si Rib Waveguides and Multimode Interferometers," IEEE Photon. Technol. Lett. 27(10), 1040-1043 (2015).
24. B. Troia, J. Soler Penades, A. Z. Khokhar, M. Nedeljkovic, C. Alonso-Ramos, V. M. N. Passaro, G. Z. Mashanovich, "Germanium-on-silicon Vernier-effect photon microcavities for the mid-infrared," Optics Letters, 41(3), 610-613 (2016).
25. M. Brun, P. Labeye, G. Grand, J. M. Hartmann, F. Boulila, M. Carras, and S. Nicoletti ,"Low loss SiGe graded index waveguides for mid-IR applications," Optics express, 22, 508 (2014).
26. L. Carletti, P. Ma, Y. Yu, B. Luther-Davies, D. Hudson, C. Monat, R. Orobtchouk, S.Madden, D.J. Moss, M.Brun, S. Ortiz, P. Labeye, S.Nicoletti, and C. Grillet, "Nonlinear optical response of low loss silicon germanium waveguides in the mid-infrared," Optics express, 23, 8261 (2015).
27. L. Carletti, M. Sinobad, P. Ma, Y. Yu, D. Allioux, R. Orobtchouk, M. Brun, S. Ortiz, P. Labeye, J. M. Hartmann, S. Nicoletti, S. Madden, B. Luther-Davies, D. J. Moss, C. Monat, and C. Grillet, "Mid-infrared nonlinear optical response of Si-Ge waveguides with ultra-short optical pulses," Optics express, 23, 32202 (2015).
28. S. Marchionna, A. Virtuani, M. Acciarri, G. Isella, and H. von Kaenel, "Defect imaging of SiGe strain relaxed buffers grown by LEPECVD" Mat. Sci. Semicond. Process. 9 (4--5) 802-805 (2006).
29. P.Chaisakul, D. Marris-Morini, J. Frigerio, D. Chrastina, M. S. Rouifed, S. Cecchi, P.Crozat, G.Isella and L. Vivien ,"Integrated germanium optical interconnects on silicon substrates," Nature Photonics, 8, 482 (2014).
30. V. Vakarin, P. Chaisakul, J. Frigerio, A. Ballabio, X. Le Roux, J.R. Coudevylle, D.Bouville , D. Perez-Galacho, L.Vivien, G.Isella and D. Marris-Morini,"Sharp bends and Mach-Zehnder interferometer based on Ge-rich-SiGe waveguides on SiGe graded buffer," Optics Express, 23, 30821 (2015).